

---

# Improving Few-Shot Visual Classification with Unlabelled Examples

---

**Peyman Bateni\***  
 University of British Columbia  
 Vancouver, BC  
 pbateni@cs.ubc.ca

**Jarred Barber\***  
 Charles River Analytics  
 Cambridge, MA  
 jarred.barber@gmail.com

**Jan-Willem van de Meent**  
 Northeastern University  
 Boston, MA  
 j.vandemeent@northeastern.edu

**Frank Wood**  
 University of British Columbia  
 Vancouver, BC  
 fwood@cs.ubc.ca

## Abstract

We propose a transductive meta-learning method that uses unlabelled instances to improve few-shot image classification performance. Our approach combines a regularized Mahalanobis-distance-based soft k-means clustering procedure with a state of the art neural adaptive feature extractor to achieve improved test-time classification accuracy using unlabelled data. We evaluate our method on transductive few-shot learning tasks, in which the goal is to jointly predict labels for query (test) examples given a set of support (training) examples. We achieve new state of the art in-domain performance on Meta-Dataset, and improve accuracy on mini- and tiered-ImageNet as compared to other conditional neural adaptive methods that use the same pre-trained feature extractor.

## 1 Introduction

Deep learning has revolutionized visual classification, enabled in part by the development of large and diverse sets of curated training data [42; 11; 17; 38; 40]. However, in many image classification settings, millions of labelled examples are not available and techniques that can achieve sufficient classification performance with few labels are required. This has motivated research on few-shot learning [5; 47; 46; 2] where methods are developed that can learn from limited labelled data while delivering comparable performance. Given a few labelled "support" images per class, a few-shot image classifier is expected to produce labels for a given set of unlabelled "query" images. Existing approaches achieve this goal through various methods for model adaptation based on the support examples of the given task. This can range from learning new class embeddings [39; 44; 41], and amortized [33; 28] or iterative [49] partial adaptation of the feature extractor, to complete fine-tuning of the entire network end-to-end [31; 6]. Most recently, Bateni et al. [1] achieved state of the art accuracy using Simple CNAPS, a conditional neural-adaptive feature extractor with a regularized Mahalanobis-distance-based classifier that uses high-dimensional mean and covariance estimates to produce class-clusters in the feature space.

While these methods use labelled support examples for few-shot learning of visual tasks, Ren et al. [32]; Kim et al. [14], and Liu et al. [22] make additional use of unlabelled data, whether through a secondary support set of images without labels [32] or by directly taking advantage of the query images, provided all at once, as unlabelled examples [22; 14]. In our work, we focus on the latter

---

\* Authors contributed equally

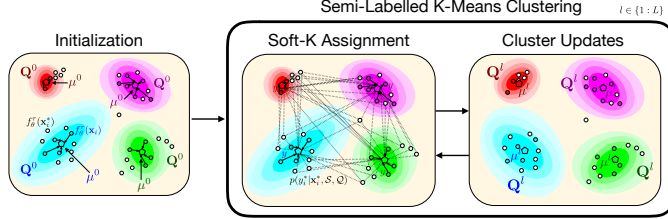


Figure 1: Soft k-means Mahalanobis-distance based clustering method used in Transductive CNAPS. First, cluster parameters are initialized using the support examples. Then, during each cluster update iteration, query examples are assigned class probabilities as soft labels and subsequently, both the soft-labelled query examples and the labelled support examples are used to produce new cluster centroids and covariance estimates.

paradigm, otherwise known as *transductive few-shot learning*. In this setting, the query examples are provided for labelling at the same time. This allows for semi-supervised learning using both support and query instances all together. Existing transductive few-shot classifiers rely on label propagation from labelled to unlabelled examples in the feature space through either k-means clustering using the squared Euclidean distance [32] or message passing in graph convolutional neural networks [22; 14].

To achieve high accuracy on few-shot visual tasks, it is crucial to use an appropriate distance metric for classification. Previous methods have used the Euclidean distance [32], the absolute difference [15], cosine similarity [44], linear classification [6; 33] or additional neural network layers [14; 41]. Simple CNAPS [1] improved these results by using a class-adaptive Mahalanobis metric. In this framework, each class is assigned a representative feature vector and a covariance metric, which is estimated from the support set. The covariance is computed using a shrinkage estimator that combines the per-class sample covariance with a global covariance and identity prior. The result is low-shot visual classification model that achieves state-of-the-art performance on the Meta-Dataset benchmark [43]. However this performance degrades in extremely low-shot regimes where five or fewer support examples are available for a given class.

Motivated by this observation, we explore the use of unlabelled examples through transductive learning of improved class covariances estimates. We show that extending Simple CNAPS with a soft k-means clustering framework can increase visual few-shot classification accuracy. Our contributions are as follows. First, we propose a transductive few-shot learner, namely Transductive CNAPS, that employs an iterative soft k-means procedure for refining class covariances using both labelled and unlabelled examples. Second, we demonstrate that when deployed at test time, an empirical improvement of 2%-3% in classification accuracy is achieved by Transductive CNAPS on the in-domain tasks on Meta-Dataset [43]. Furthermore, Transductive CNAPS outperforms CNAPS-based baselines such as Simple CNAPS [1] and CNAPS [33] by statistically significant margins on mini-ImageNet [39] and tiered-Imagenet [32].

## 2 Related work

### 2.1 Few-Shot Learning using Labelled Data

Early work on few-shot visual classification has focused on improving classification accuracy through the use of better classification metrics with a meta-learned non-adaptive feature extractor. Matching networks [44] use cosine similarities over feature vectors produced by independently learned feature extractors. Siamese networks [15] classify query images based on the nearest support example in feature space, under the  $L_1$  metric. Relation networks [41] and variants [14; 36] learn their own similarity metric, parameterised through a Multi-Layer Perceptron. More recently, Prototypical Networks [39] learn a shared feature extractor that is used to produce class means in a feature space where the Euclidean distance is used for classification.

Other work has focused on adapting the feature extractor for new tasks. Transfer learning by fine-tuning pre-trained visual classifiers [49] was an early approach that proved limited in success due to issues arising from over-fitting. MAML [6] and its variants [25; 26; 31] learn meta-parameters that allow fast task-adaptation with only a few gradient updates. More recently, work has been done on partial adaptation of feature extractors using conditional neural adaptive processes [28; 7; 33; 1]. These methods rely on channel-wise adaptation of pre-trained convolutional layers by adjusting

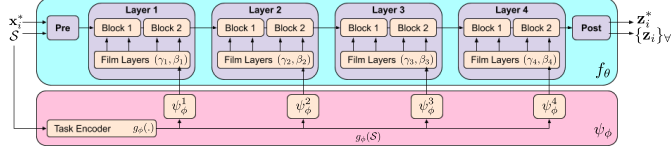


Figure 2: Overview of the neural adaptive feature extraction process used in Transductive CNAPS. Figure was adapted from [1].

parameters of FiLM layers [29] inserted throughout the network. Our work builds on the most recent of these neural adaptive approaches, specifically Simple CNAPS [1].

## 2.2 Few-Shot Learning using Unlabelled Data

In addition to labelled support examples, some approaches [14; 22; 32] in few-shot visual classification have explored the use of unlabelled instances to improve performance. EGNN [14] employs a graph convolutional edge-labelling network for iterative propagation of labels from support to query instances. Similarly, TPN [22] learns a graph construction module for neural propagation of soft labels for transductive inference on the query set. These methods rely on a neural parameterization of distance within the feature space. Finally, [32] proposed a soft k-means approach (extending Prototypical Networks [39]) that uses a single soft-weighted update to learn class prototypes.

## 3 Method

### 3.1 Problem Definition

Following [39; 1; 33; 6], we focus on a few-shot classification setting where a distribution  $D$  over image classification tasks  $(\mathcal{S}, \mathcal{Q})$  is provided for training. Each task  $(\mathcal{S}, \mathcal{Q}) \sim D$  consists of a support set  $\mathcal{S} = \{(\mathbf{x}_i, y_i)\}_{i=1}^n$  of labelled images and a query set  $\mathcal{Q} = \{\mathbf{x}_i^*\}_{i=1}^m$  of unlabelled images; the goal is to predict labels for these query examples, given the (typically small) support set. Each query image  $\mathbf{x}_i^* \in \mathcal{Q}$  has a corresponding ground truth label  $y_i^*$  available at training time. A model will be trained by maximizing, over some parameters  $\theta$  (which are shared across tasks), the expected query set classification loss over tasks:  $\mathbb{E}_{(\mathcal{S}, \mathcal{Q}) \sim D} [\sum_{\mathbf{x}_i^* \in \mathcal{Q}} \log p_\theta(y_i^* | \mathbf{x}_i^*, \mathcal{S}, \mathcal{Q})]$ ; the inclusion of the dependence on all of  $\mathcal{Q}$  here allows for the model to be transductive. At test time, a separate distribution of tasks generated from previously unseen images and classes is used to evaluate performance. We also define *shot* as the number of support examples per class, and *way* as the number of classes within the task.

### 3.2 Simple CNAPS

Our method extends the Simple CNAPS[1] architecture for few-shot visual classification. Simple CNAPS performs few-shot classification in two steps. First, it computes task-adapted features for every support and query example. This part of the architecture is the same as that in CNAPS [33], and is based on the FiLM metalearning framework[29]. Second, it uses the support set to estimate a per-class Mahalanobis metric, which is used to assign query examples to classes.

Figure 3 shows a comparison between Simple CNAPS and Transductive CNAPS, the architecture that we develop in this paper. Both architectures use a ResNet18[11] feature extractor, pre-trained on ImageNet [34], denoted as  $\tilde{f}_\theta$ . Within each residual block, Feature-wise Linear Modulation (FiLM) layers compute a scale factor  $\gamma$  and shift  $\beta$  for each output channel, using block-specific adaptation networks  $\psi_\phi$  that are conditioned on a task encoding  $g_\phi(\mathcal{S})$ . This produces an adapted feature extractor  $f_\theta$  (which implicitly depends on the support set  $\mathcal{S}$ ) that maps support/query images onto the corresponding adapted feature space. We will denote by  $\mathcal{S}_\theta, \mathcal{Q}_\theta$  versions of the support/query sets where each image is mapped into its feature representation  $\mathbf{z} = f_\theta(\mathbf{x})$ .

Where Simple CNAPS and Transductive CNAPS differ is in how they construct the classifier. Simple CNAPS computes a Mahalanobis distance relative to each class  $k$  by estimating a mean  $\mu_k$  and regularized covariance  $\mathbf{Q}_k$  in the adapted feature space, using the support instances:

$$\mu_k = \frac{1}{n_k} \sum_i \mathbb{I}[y_i = k] \mathbf{z}_i, \quad \mathbf{Q}_k = \lambda_k \Sigma_k + (1 - \lambda_k) \Sigma + \beta I, \quad \lambda_k = \frac{n_k}{n_k + 1}. \quad (1)$$

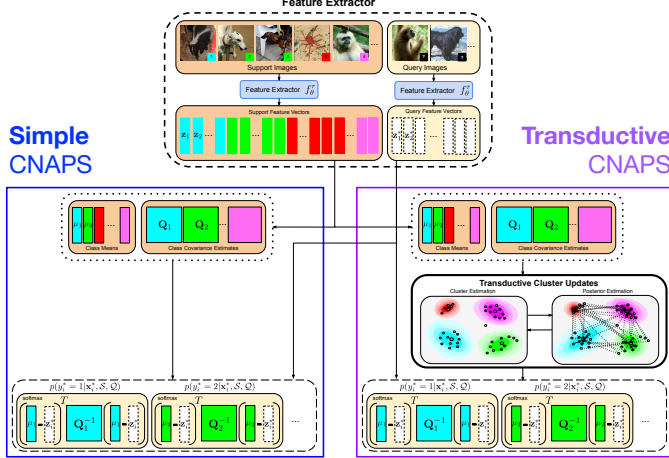


Figure 3: Transductive CNAPS (right) extends the Mahalanobis-distance based classifier in Simple CNAPS (left) through transductive soft k-means clustering of the visual space.

Here  $\mathbb{I}[y_i = k]$  is the indicator function and  $n_k = \sum_i \mathbb{I}[y_i = k]$  is the number of examples with class  $k$  in the support set  $\mathcal{S}$ . The ratio  $\lambda_k$  balances an task-conditional sample covariance  $\Sigma$  and a class-conditional sample covariance  $\Sigma_k$ :

$$\Sigma = \frac{1}{n} \sum_i (\mathbf{z}_i - \mu) (\mathbf{z}_i - \mu)^T, \quad \Sigma_k = \frac{1}{n_k} \sum_i \mathbb{I}[y_i = k] (\mathbf{z}_i - \mu_k) (\mathbf{z}_i - \mu_k)^T, \quad (2)$$

where  $\mu = \frac{1}{n} \sum_i \mathbf{z}_i$  is the task-level mean. When few support examples are available for a particular class,  $\lambda_k$  is small, and the estimate is regularized towards the task-level covariance  $\Sigma$ . As the number of support examples for the class increases, the estimate tends to towards the class-conditional covariance  $\Sigma_k$ . Additionally, an identity regularizer  $\beta I$  is added to the covariance estimate to ensure invertability of the covariance matrix.

Given the class means and covariances, Simple CNAPS computes class probabilities for each query feature vector  $\mathbf{z}_i^*$  by as a softmax over the squared Mahalanobis distances with respect to each class:

$$p(y^* = k | \mathbf{z}^*) \propto \exp \left( -(\mathbf{z} - \mu_k)^T \mathbf{Q}_k^{-1} (\mathbf{z} - \mu_k) \right). \quad (3)$$

### 3.3 Transductive CNAPS

We can interpret Simple CNAPS as a form of supervised clustering in feature space; each cluster (corresponding to a class  $k$ ) is parameterized with a centroid  $\mu_k$  and a metric  $\mathbf{Q}_k$ , and we interpret (3) as class assignment probabilities based on the distance to each centroid.

With this viewpoint in mind, a natural extension to consider is to use the estimates of the class assignment probabilities on unlabelled data to refine the class parameters  $\mu_k$ ,  $\mathbf{Q}_k$  in a soft  $k$ -means framework based on per-cluster Mahalanobis distances [24]. In this framework, we alternate between computing updated assignment probabilities using (3) on the query set and using those assignment probabilities to compute updated class parameters.

We will define  $\mathcal{R}_\theta = \mathcal{S}_\theta \sqcup \mathcal{Q}_\theta$  as the disjoint union of the support set and the query set. For each element of  $\mathcal{R}_\theta$ , which we index by  $j$ , we define responsibilities  $w_{jk}$  in terms of their class predictions when it is part of the query set and in terms of the label when it is part of the support set,

$$w_{jk} = \begin{cases} p(y'_j = k | \mathbf{z}'_j) & \mathbf{z}'_j \in \mathcal{Q}_\theta, \\ \mathbb{I}[y'_j = k] & (\mathbf{z}'_j, y'_j) \in \mathcal{S}_\theta. \end{cases} \quad (4)$$

Using these responsibilities we can incorporate unlabelled samples from the support set by defining weighted estimates  $\mu'_k$  and  $\mathbf{Q}'_k$ :

$$\mu'_k = \frac{1}{n'_k} \sum_j w_{jk} \mathbf{z}'_j \quad \mathbf{Q}'_k = \lambda'_k \Sigma'_k + (1 - \lambda'_k) \Sigma' + \beta I, \quad (5)$$

---

**Algorithm 1** Iterative Refinement in Transductive-CNAPS

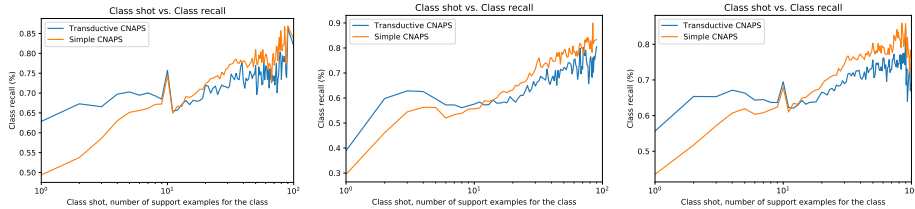
---

```

1: procedure COMPUTE_QUERY_LABELS( $\mathcal{S}_\theta, \mathcal{Q}_\theta, N_{\text{iter}}$ )
2:   For  $j$  ranging over support and query sets,  $w_{jk} \leftarrow \begin{cases} 1 & \text{if } (\mathbf{z}'_j, y'_j) \in \mathcal{S}_\theta \text{ and } y_j = k \\ 0 & \text{otherwise} \end{cases}$ 
3:   for  $\text{iter} = 0 \dots N_{\text{iter}}$  do ▷ The first iteration is equivalent to Simple CNAPS;
4:     Compute class parameters  $\mu_k, \mathbf{Q}_k$  according to update equations (5)-(6)
5:     Compute class weights using class parameters according to (4)
6:     break if the most probable class for each query example hasn't changed
7:   end for
8:   return class probabilities  $w_{jk}$  for  $j$  corresponding to  $\mathcal{Q}_\theta$ 
9: end procedure

```

---



(a) In-Domain Recall vs. *Shot* (b) Out-Domain Recall vs. *Shot* (c) Overall Recall vs. *Shot*

Figure 4: Class recall (otherwise noted as in-class query accuracy) averaged between classes across all tasks and (a: In-Domain, b: Out-of-domain, c: all) Meta-Dataset datasets. Class recalls have been grouped together, averaged and plotted according to the class *shot* in (a), (b), and (c).

where  $n'_k = \sum_j w_{jk}$  defines  $\lambda'_k = n'_k / (n'_k + 1)$ , and the covariance estimates  $\Sigma'$  and  $\Sigma'_k$  are

$$\Sigma' = \frac{1}{\sum_k n'_k} \sum_{jk} w_{jk} (\mathbf{z}'_j - \mu') (\mathbf{z}'_j - \mu')^T, \quad \Sigma'_k = \frac{1}{n'_k} \sum_j w_{jk} (\mathbf{z}'_j - \mu'_k) (\mathbf{z}'_j - \mu'_k)^T. \quad (6)$$

with  $\mu' = (\sum_k n'_k)^{-1} \sum_{jk} w_{jk} \mathbf{z}'_j$  being the task-level mean. These update equations are simply weighted versions of the original Simple CNAPS estimators from Section 3.2, and reduce to them exactly in the case of an empty query set.

Algorithm 1 summarizes the soft k-means procedure based on these updates. We initialize our weights using only the labelled support set. We use those weights to compute class parameters, then compute updated weights using both the support and query sets. At this point, the weights associated with the query set  $\mathcal{Q}$  are the same class probabilities as estimated by Simple CNAPS. However, we continue this procedure iteratively until we reach either reach a maximum number of iterations, or until class assignments  $\text{argmax}_k w_{jk}$  stop changing.

## 4 Experiments

### 4.1 Benchmarks

**Meta-Dataset** [43] is a few-shot image classification benchmark that consists of 10 widely used datasets: ILSVRC-2012 (ImageNet) [34], Omniglot [18], FGVC-Aircraft (Aircraft) [23], CUB-200-2011 (Birds) [45], Describable Textures (DTD) [4], QuickDraw [13], FGVCx Fungi (Fungi) [37], VGG Flower (Flower) [27], Traffic Signs (Signs) [12] and MSCOCO [21]. Consistent with past work [33; 1], we train our model on the official training splits of the first 8 datasets and use the test splits to evaluate in-domain performance. We use the remaining two dataset as well as three external benchmarks, namely MNIST [19], CIFAR10 [16] and CIFAR100 [16], for out-of-domain evaluation.

Task generation in Meta-Dataset follows a complex procedure where tasks can be of different *ways* and individual classes can be of varying *shots* even within the same task. Specifically, for each task, the task *way* is first sampled uniformly between 5 and 50 and *way* classes are selected at random from the corresponding class/dataset split. Then, for each class, 10 instances are sampled at random and used as query examples for the class, while of the remaining images for the class, a *shot* is sampled

Model	In-Domain Accuracy (%)							
	ImageNet	Omniglot	Aircraft	Birds	DTD	QuickDraw	Fungi	Flower
MAML [6]	32.4±1.0	71.9±1.2	52.8±0.9	47.2±1.1	56.7±0.7	50.5±1.2	21.0±1.0	70.9±1.0
RelationNet [41]	30.9±0.9	86.6±0.8	69.7±0.8	54.1±1.0	56.6±0.7	61.8±1.0	32.6±1.1	76.1±0.8
k-NN [43]	38.6±0.9	74.6±1.1	65.0±0.8	66.4±0.9	63.6±0.8	44.9±1.1	37.1±1.1	83.5±0.6
MatchingNet [44]	36.1±1.0	78.3±1.0	69.2±1.0	56.4±1.0	61.8±0.7	60.8±1.0	33.7±1.0	81.9±0.7
Finetune [49]	43.1±1.1	71.1±1.4	72.0±1.1	59.8±1.2	<b>69.1±0.9</b>	47.1±1.2	38.2±1.0	85.3±0.7
ProtoNet [39]	44.5±1.1	79.6±1.1	71.1±0.9	67.0±1.0	65.2±0.8	64.9±0.9	40.3±1.1	86.9±0.7
ProtoMAML [43]	47.9±1.1	82.9±0.9	74.2±0.8	70.0±1.0	<b>67.9±0.8</b>	66.6±0.9	42.0±1.1	88.5±0.7
CNAPS [33]	51.3±1.0	88.0±0.7	76.8±0.8	71.4±0.9	62.5±0.7	71.9±0.8	46.0±1.1	89.2±0.5
AR-CNAPS [33]	52.3±1.0	88.4±0.7	80.5±0.6	72.2±0.9	58.3±0.7	72.5±0.8	47.4±1.0	86.0±0.5
Simple CNAPS [1]	<b>58.6±1.1</b>	91.7±0.6	82.4±0.7	74.9±0.8	<b>67.8±0.8</b>	<b>77.7±0.7</b>	46.9±1.0	90.7±0.5
Transductive CNAPS	<b>58.8±1.1</b>	<b>95.2±0.3</b>	<b>84.0±0.6</b>	<b>76.4±0.7</b>	<b>68.5±0.8</b>	<b>77.8±0.7</b>	<b>49.7±1.0</b>	<b>92.7±0.4</b>

Table 1: In-domain few-shot classification accuracy of Transductive CNAPS compared to previous methods. With the exception of [AR-]CNAPS and Simple CNAPS where the reported results come from [33] and [1], all other benchmarks are reproduced directly from [43]. Error intervals showcase 95% confidence intervals on the reported performances across the 600 evaluated tasks per each dataset. Values in bold achieve state of the art performance with statistically significant margins.

Model	Out-of-Domain Accuracy (%)					Average Accuracy (%)		
	Signs	MSCOCO	MNIST	CIFAR10	CIFAR100	In-Domain	Out-Domain	Overall
MAML [6]	34.2±1.3	24.1±1.1	NA	NA	NA	50.4±1.0	29.2±1.2	46.2±1.1
RelationNet [41]	37.5±0.9	27.4±0.9	NA	NA	NA	58.6±0.9	32.5±0.9	53.3±0.9
k-NN [43]	40.1±1.1	29.6±1.0	NA	NA	NA	59.2±0.9	34.9±1.1	54.3±0.9
MatchingNet [44]	55.6±1.1	28.8±1.0	NA	NA	NA	59.8±0.9	42.2±1.1	56.3±1.0
Finetune [49]	66.7±1.2	35.2±1.1	NA	NA	NA	60.7±1.1	51.0±1.2	58.8±1.1
ProtoNet [39]	46.5±1.0	39.9±1.1	74.3±0.8	66.4±0.7	54.7±1.1	64.9±1.0	56.4±0.9	61.6±0.9
ProtoMAML [43]	52.3±1.1	41.3±1.0	NA	NA	NA	67.5±0.9	46.8±1.1	63.4±0.9
CNAPS [33]	60.1±0.9	42.3±1.0	88.6±0.5	60.0±0.8	48.1±1.0	69.6±0.8	59.8±0.8	65.9±0.8
AR-CNAPS [33]	60.2±0.9	42.9±1.1	92.7±0.4	61.5±0.7	50.1±1.0	69.7±0.8	61.5±0.8	66.5±0.8
Simple CNAPS [1]	<b>73.5±0.7</b>	<b>46.2±1.1</b>	<b>93.9±0.4</b>	<b>74.3±0.7</b>	<b>60.5±1.0</b>	73.8±0.8	<b>69.7±0.8</b>	<b>72.2±0.8</b>
Transductive CNAPS	70.8±0.7	<b>47.3±1.0</b>	<b>94.2±0.4</b>	<b>75.2±0.7</b>	<b>61.2±1.0</b>	<b>75.4±0.7</b>	<b>69.7±0.8</b>	<b>73.2±0.7</b>

Table 2: Middle) Out-of-domain few-shot classification accuracy and (Right) in-domain, out-of-domain and overall mean accuracy of Transductive CNAPS compared to past methods. With the exception of [AR-]CNAPS and Simple CNAPS where the reported results come from [33] and [1], all other benchmarks are reproduced directly from [43]. Error intervals showcase 95% confidence intervals on the reported performances across the 600 evaluated tasks per each dataset. Values in bold achieve state of the art performance with statistically significant margins.

uniformly from [1, 100] and *shot* number of images are selected at random as support examples with total support set size of 500. Additional dataset-specific constraints are enforced, as discussed in Section 3.2 of [43], and since some datasets have fewer than 50 classes and fewer than 100 images per class, the overall *way* and *shot* distributions resemble Poisson distributions where most tasks have fewer than 10 classes and most classes have fewer than 10 support examples (see Appendix-A.1). We train for a total of 110K tasks using Episodic Training [39; 6] (see Appendix-A.3 for details).

**mini/tiered-ImageNet** [44; 32] are two benchmarks for few-shot learning. Both datasets employ subsets of ImageNet [34] with a total of 100 classes and 60K images in mini-ImageNet and 608 classes and 779K images in tiered-ImageNet. Unlike Meta-Dataset, tasks across these datasets have pre-defined *shots/ways* that are uniform across every task generated in the specified setting. Following [26; 22; 39], we report performance on the 1/5-*shot* 5/10-*way* settings across both datasets with 10 query examples per class. We train episodically for 20K tasks (see Appendix-A.2 for details).

## 4.2 Results

**Evaluation on Meta-Dataset:** In-domain, out-of-domain and overall accuracy on the Meta-Dataset are shown in Tables 1/2. Transductive CNAPS sets new state of the art accuracy on 5 out of the 8

Model	mini-ImageNet Accuracy (%)				tiered-ImageNet Accuracy (%)			
	5-way		10-way		5-way		10-way	
	1-shot	5-shot	1-shot	5-shot	1-shot	5-shot	1-shot	5-shot
CNAPS [33]	77.8 $\pm$ 1.0	87.6 $\pm$ 0.7	65.7 $\pm$ 0.7	80.0 $\pm$ 0.6	75.7 $\pm$ 1.0	85.5 $\pm$ 0.7	63.7 $\pm$ 0.7	78.2 $\pm$ 0.5
Simple CNAPS [1]	80.5 $\pm$ 0.9	89.5 $\pm$ 0.6	68.6 $\pm$ 0.7	83.7 $\pm$ 0.5	79.0 $\pm$ 0.9	87.6 $\pm$ 0.6	67.1 $\pm$ 0.7	81.0 $\pm$ 0.5
Transductive CNAPS	<b>82.4<math>\pm</math>0.9</b>	<b>90.9<math>\pm</math>0.5</b>	<b>73.3<math>\pm</math>0.7</b>	<b>85.7<math>\pm</math>0.5</b>	<b>81.0<math>\pm</math>0.9</b>	<b>89.2<math>\pm</math>0.6</b>	<b>69.1<math>\pm</math>0.7</b>	<b>83.1<math>\pm</math>0.5</b>

Table 3: Few-shot visual classification results on 1/5-shot 5/10-way few-shot on mini/tiered-ImageNet. Note that all results were re-produced using the same generated tasks for consistency in comparison. Intervals showcase 95% confidence intervals on the reported performances across the 600 evaluated tasks per each setting. Values in bold achieve statistically meaningful state of the art performance. All reported accuracies are averaged between five distinct runs.

Model	In-Domain Accuracy (%)								
	ImageNet	Omniglot	Aircraft	Birds	DTD	QuickDraw	Fungi	Flower	
GMM-EM+ CNAPS	46.4 $\pm$ 0.9	86.6 $\pm$ 0.8	73.8 $\pm$ 0.7	68.8 $\pm$ 0.8	57.5 $\pm$ 0.7	61.7 $\pm$ 0.8	35.9 $\pm$ 0.9	84.2 $\pm$ 0.6	
GMM CNAPS	45.3 $\pm$ 1.0	88.0 $\pm$ 0.9	80.8 $\pm$ 0.8	71.4 $\pm$ 0.8	61.1 $\pm$ 0.7	70.7 $\pm$ 0.8	42.9 $\pm$ 1.0	88.1 $\pm$ 0.6	
GMM-EM CNAPS	48.7 $\pm$ 1.0	92.3 $\pm$ 0.5	80.0 $\pm$ 0.7	72.4 $\pm$ 0.7	59.8 $\pm$ 0.7	71.1 $\pm$ 0.7	41.4 $\pm$ 0.9	87.7 $\pm$ 0.5	
Transductive+ CNAPS	55.3 $\pm$ 1.1	92.2 $\pm$ 0.5	79.9 $\pm$ 0.7	72.3 $\pm$ 0.9	<b>74.3<math>\pm</math>0.7</b>	72.7 $\pm$ 0.9	42.3 $\pm$ 1.0	<b>92.0<math>\pm</math>0.4</b>	
Simple CNAPS [1]	<b>58.6<math>\pm</math>1.1</b>	91.7 $\pm$ 0.6	82.4 $\pm$ 0.7	74.9 $\pm$ 0.8	67.8 $\pm$ 0.8	<b>77.7<math>\pm</math>0.7</b>	46.9 $\pm$ 1.0	90.7 $\pm$ 0.5	
Transductive CNAPS	<b>58.8<math>\pm</math>1.1</b>	<b>95.2<math>\pm</math>0.3</b>	<b>84.0<math>\pm</math>0.6</b>	<b>76.4<math>\pm</math>0.7</b>	68.5 $\pm$ 0.8	<b>77.8<math>\pm</math>0.7</b>	<b>49.7<math>\pm</math>1.0</b>	<b>92.7<math>\pm</math>0.4</b>	

Table 4: In-domain few-shot classification accuracy of Transductive(+) CNAPS compared to GMM-based ablations. Error intervals showcase 95% confidence intervals on the report performances across the 600 evaluated tasks per dataset. Values in bold achieve state of the art performance with statistically significant margins.

in-domain datasets, while matching past methods on the remaining 3. On out-of-domain tasks, it matches Simple CNAPS on 4 out of the 5 datasets, while performing worse on Signs. We attribute this to the dataset’s highly specialized domain which makes transductive learning more difficult. Overall, Transductive+ CNAPS achieves 75.4% $\pm$ 0.7%, 69.7% $\pm$ 0.8%, and 73.2% $\pm$ 0.7% on in-domain, out-of-domain and overall mean accuracy, outperforming past state of the art on in-domain datasets while statistically matching Simple CNAPS on out-of-domain datasets and overall mean performance.

**Evaluation on mini/tiered-ImageNet:** As shown in Table 3, Transductive CNAPS achieves better performance as compared to CNAPS and Simple CNAPS on 1/5-shot 5/10-way few-shot classification on both mini/tiered-ImageNet. We explicitly omit other baselines (instead provided in Appendix-B), as although our model outperforms them, CNAPS-derived methods use an feature extractor pre-trained on ImageNet, which gives them an unfair advantage on ImageNet-based benchmarks.

**Performance vs. Class Shot:** In Figure 4, we examine the relationship between class recall (i.e. classification accuracy among query examples belonging to the class itself) and the number of support examples given for the class (*shot*). As demonstrated, Transductive CNAPS is especially effective when class *shot* is below 10, showing large average recall improvements, especially at the 1-*shot* level. However, as the class *shot* increases beyond 10, we see performance loss compared to Simple CNAPS. This suggests that soft k-means learning of cluster parameters can be effective when very few support examples are otherwise available for use. Conversely, in high-*shot* classes, the transductive updates may act as distractions. We also observe that the margin of improvement on low-*shot* classes is diminished on out-of-domain tasks as compared to in-domain. This signifies the importance of properly adapting the feature space, a task that is more difficult to perform on out-of-domain tasks, and its impact on the effectiveness of our method.

**Training Transductive CNAPS:** In our work, we use Transductive CNAPS at test-time only, using a pre-trained Simple CNAPS feature adaptation network. It’s natural to consider training the feature adaptation network end-to-end through the soft k-means transduction procedure. We provide this comparison in the bottom-halves of Tables 4 and 5 where Transductive+ CNAPS describes this end-to-end trained setting. End-to-end training results in an average accuracy decrease of 2.5%, which we hypothesize to be due to the difficulty of learning with transductive soft-labels that are noisy especially in the early iterations.

Model	Out-of-Domain Accuracy (%)					Average Accuracy (%)		
	Sigs	MSCOCO	MNIST	CIFAR10	CIFAR100	In-Domain	Out-Domain	Overall
GMM-EM+ CNAPS	56.7±0.9	37.4±0.8	89.8±0.4	58.9±0.8	43.7±0.8	64.4±0.8	57.3±0.7	61.6±0.8
GMM CNAPS	68.9±0.7	37.2±0.9	91.4±0.5	64.5±0.7	46.6±0.9	68.5±0.8	61.7±0.7	65.9±0.8
GMM-EM CNAPS	63.6±0.8	39.2±0.8	89.8±0.5	66.9±0.7	50.5±0.8	69.2±0.7	62.0±0.7	66.4±0.7
Transductive+ CNAPS	67.5±0.8	<b>45.8±1.1</b>	<b>95.6±0.3</b>	73.0±0.7	55.8±1.1	72.6±0.8	67.5±0.8	70.7±0.8
Simple CNAPS [1]	<b>73.5±0.7</b>	<b>46.2±1.1</b>	93.9±0.4	<b>74.3±0.7</b>	<b>60.5±1.0</b>	73.8±0.8	<b>69.7±0.8</b>	<b>72.2±0.8</b>
Transductive CNAPS	70.8±0.7	<b>47.3±1.0</b>	94.2±0.4	<b>75.2±0.7</b>	<b>61.2±1.0</b>	<b>75.4±0.7</b>	<b>69.7±0.8</b>	<b>73.2±0.7</b>

Table 5: Middle) Out-of-domain few-shot classification accuracy and (Right) in-domain, out-of-domain and overall mean accuracy of Transductive(+) CNAPS compared to GMM-based ablations. Error intervals showcase 95% confidence intervals on the report performances across the 600 evaluated tasks per dataset. Values in bold achieve statistically significant state of the art performance.

**Comparison to Gaussian Mixture Models:** The Mahalanobis-distance based class probabilities produced by Equation 3 closely resembles the cluster posterior probabilities (responsibilities) inferred by a Gaussian Mixture Model (GMM). The only changes required to make this correspondence exact is to introduce a class prior distribution  $\pi$ , and to change the class probability model (3) to the Gaussian likelihood:

$$p(y^* = k \mid \mathbf{z}^*) \propto \exp \left( -\frac{1}{2}(\mathbf{z} - \mu_k)^T \mathbf{Q}_k^{-1} (\mathbf{z} - \mu_k) - \frac{1}{2} \log |\mathbf{Q}_k| \right) \quad (7)$$

With these modifications, Transductive CNAPS would exactly correspond to inference in a GMM, with cluster parameters learned through semi-supervised expectation maximization (EM). Given this observation, we consider three ablations that use this inference model: First, GMM CNAPS, which is equivalent to Simple CNAPS using GMM inference instead (no EM); second, GMM-EM CNAPS, which extends GMM CNAPS by performing test-time EM (the iterative refinement in Algorithm 1, with the correct GMM likelihood); and lastly, GMM+EM+ CNAPS, which uses GMM-EM CNAPS with EM performed during training as well. These three models, in order, correspond to GMM versions of Simple CNAPS, Transductive CNAPS and the Transductive+ CNAPS ablation discussed. We provide results on these GMM-based ablations in the upper-halves of Tables 4 and 5. Surprisingly, the addition of the  $\log(\det(\mathbf{Q}_k))$  term results in 6%-9% loss in classification accuracy.

However, when the Gaussian likelihoods within the GMMs are not properly normalized, higher classification accuracy can be achieved. We also observe that transductive learning in GMM-based CNAPS models through semi-supervised EM improves accuracy at test-time, but reduces performance when used during training as well. These trends are similar to our results for Transductive CNAPS.

## 5 Discussion

In this paper, we have presented a few-shot visual classification method that achieves new state of the art performance via a transductive clustering procedure for refining class parameters derived from a previous neural adaptive Mahalanobis-distance based approach. The resulting architecture, Transductive CNAPS, is more effective at producing useful estimates of class mean and covariance especially in low-shot settings, when used at test time. Even though we demonstrate the efficacy of our approach in the transductive domain where query examples themselves are used as unlabelled data, our soft k-means clustering procedure can naturally extend to use other sources of unlabelled examples in a semi-supervised fashion.

Transductive CNAPS superficially resembles a transductive GMM model stacked on top of a learned feature representation; however, when we try to make this connection exact, we suffer substantial performance hits. This suggests that the appropriate framework to reason about the Transductive CNAPS and Simple CNAPS family of models is through local metric learning [30; 48; 10]; the class precision matrices  $\mathbf{Q}_k^{-1}$  play the role of the Riemannian metric at the class centroids, and the resulting classifier is a coarse approximation of a distance-based classifier on the induced Riemannian manifold. We discuss this connection in more depth in Appendix C. Working out the exact nature of the geometric connection, and why the probabilistic model fails empirically, is a subject for future research.

## 6 Acknowledgments

We acknowledge the support of the Natural Sciences and Engineering Research Council of Canada (NSERC), the Canada Research Chairs (CRC) Program, the Canada CIFAR AI Chairs Program, Compute Canada, Intel, and DARPA under its D3M and LWLL programs. Additionally, this material is based upon work supported by the United States Air Force under Contract No. FA8750-19-C-0515.

## References

- [1] Peyman Bateni, Raghav Goyal, Vaden Masrani, Frank Wood, and Leonid Sigal. Improved few-shot visual classification. 2019.
- [2] Aurélien Bellet, Amaury Habrard, and Marc Sebban. A survey on metric learning for feature vectors and structured data. *arXiv preprint arXiv:1306.6709*, 2013.
- [3] Manfredo Perdigao do Carmo. *Riemannian geometry*. Birkhäuser, 1992.
- [4] Mircea Cimpoi, Subhransu Maji, Iasonas Kokkinos, Sammy Mohamed, and Andrea Vedaldi. Describing textures in the wild. In *Proceedings of the IEEE Conference on Computer Vision and Pattern Recognition*, pages 3606–3613, 2014.
- [5] Abdur R Feyjie, Reza Azad, Marco Pedersoli, Claude Kauffman, Ismail Ben Ayed, and Jose Dolz. Semi-supervised few-shot learning for medical image segmentation, 2020.
- [6] Chelsea Finn, Pieter Abbeel, and Sergey Levine. Model-agnostic meta-learning for fast adaptation of deep networks. In *Proceedings of the 34th International Conference on Machine Learning-Volume 70*, pages 1126–1135. JMLR. org, 2017.
- [7] Marta Garnelo, Dan Rosenbaum, Chris J. Maddison, Tiago Ramalho, David Saxton, Murray Shanahan, Yee Whye Teh, Danilo J. Rezende, and S. M. Ali Eslami. Conditional neural processes. *CoRR*, abs/1807.01613, 2018. URL <http://arxiv.org/abs/1807.01613>.
- [8] Spyros Gidaris and Nikos Komodakis. Dynamic few-shot visual learning without forgetting. *CoRR*, abs/1804.09458, 2018. URL <http://arxiv.org/abs/1804.09458>.
- [9] Will Grathwohl, Kuan-Chieh Wang, Jörn-Henrik Jacobsen, David Duvenaud, Mohammad Norouzi, and Kevin Swersky. Your classifier is secretly an energy based model and you should treat it like one. *ICLR 2020*, 2020.
- [10] Søren Hauberg, Oren Freifeld, and Michael J Black. A geometric take on metric learning. In *Advances in Neural Information Processing Systems*, pages 2024–2032, 2012.
- [11] Kaiming He, Xiangyu Zhang, Shaoqing Ren, and Jian Sun. Deep residual learning for image recognition. *CoRR*, abs/1512.03385, 2015. URL <http://arxiv.org/abs/1512.03385>.
- [12] Sebastian Houben, Johannes Stallkamp, Jan Salmen, Marc Schlipsing, and Christian Igel. Detection of traffic signs in real-world images: The german traffic sign detection benchmark. In *The 2013 international joint conference on neural networks (IJCNN)*, pages 1–8. IEEE, 2013.
- [13] Jonas Jongejan, Henry Rowley, Takashi Kawashima, Jongmin Kim, and Nick Fox-Gieg. The quick, draw!-ai experiment.(2016), 2016.
- [14] Jongmin Kim, Taesup Kim, Sungwoong Kim, and Chang D. Yoo. Edge-labeling graph neural network for few-shot learning. *CoRR*, abs/1905.01436, 2019. URL <http://arxiv.org/abs/1905.01436>.
- [15] Gregory Koch, Richard Zemel, and Ruslan Salakhutdinov. Siamese neural networks for one-shot image recognition. In *ICML deep learning workshop*, volume 2, 2015.
- [16] Alex Krizhevsky. Learning multiple layers of features from tiny images. Technical report, 2009.
- [17] Alex Krizhevsky, Ilya Sutskever, and Geoffrey E. Hinton. Imagenet classification with deep convolutional neural networks. *Commun. ACM*, 60(6):84–90, May 2017. ISSN 0001-0782. doi: 10.1145/3065386. URL <http://doi.acm.org/10.1145/3065386>.

[18] Brenden M Lake, Ruslan Salakhutdinov, and Joshua B Tenenbaum. Human-level concept learning through probabilistic program induction. *Science*, 350(6266):1332–1338, 2015.

[19] Yann LeCun and Corinna Cortes. MNIST handwritten digit database. 2010. URL <http://yann.lecun.com/exdb/mnist/>.

[20] John M Lee. Smooth manifolds. In *Introduction to Smooth Manifolds*, pages 1–31. Springer, 2013.

[21] Tsung-Yi Lin, Michael Maire, Serge Belongie, James Hays, Pietro Perona, Deva Ramanan, Piotr Dollár, and C Lawrence Zitnick. Microsoft coco: Common objects in context. In *European conference on computer vision*, pages 740–755. Springer, 2014.

[22] Yanbin Liu, Juho Lee, Minseop Park, Saehoon Kim, and Yi Yang. Transductive propagation network for few-shot learning. *CoRR*, abs/1805.10002, 2018. URL <http://arxiv.org/abs/1805.10002>.

[23] Subhransu Maji, Esa Rahtu, Juho Kannala, Matthew Blaschko, and Andrea Vedaldi. Fine-grained visual classification of aircraft. *arXiv preprint arXiv:1306.5151*, 2013.

[24] Igor Melnykov and Volodymyr Melnykov. On k-means algorithm with the use of mahalanobis distances. *Statistics & Probability Letters*, 84:88–95, 2014.

[25] Nikhil Mishra, Mostafa Rohaninejad, Xi Chen, and Pieter Abbeel. Meta-learning with temporal convolutions. *CoRR*, abs/1707.03141, 2017. URL <http://arxiv.org/abs/1707.03141>.

[26] Alex Nichol, Joshua Achiam, and John Schulman. On first-order meta-learning algorithms. *CoRR*, abs/1803.02999, 2018. URL <http://arxiv.org/abs/1803.02999>.

[27] Maria-Elena Nilsback and Andrew Zisserman. Automated flower classification over a large number of classes. In *2008 Sixth Indian Conference on Computer Vision, Graphics & Image Processing*, pages 722–729. IEEE, 2008.

[28] Boris Oreshkin, Pau Rodríguez López, and Alexandre Lacoste. Tadam: Task dependent adaptive metric for improved few-shot learning. In S. Bengio, H. Wallach, H. Larochelle, K. Grauman, N. Cesa-Bianchi, and R. Garnett, editors, *Advances in Neural Information Processing Systems 31*, pages 721–731. Curran Associates, Inc., 2018. URL <http://papers.nips.cc/paper/7352-tadam-task-dependent-adaptive-metric-for-improved-few-shot-learning.pdf>.

[29] Ethan Perez, Florian Strub, Harm De Vries, Vincent Dumoulin, and Aaron Courville. Film: Visual reasoning with a general conditioning layer. In *Thirty-Second AAAI Conference on Artificial Intelligence*, 2018.

[30] Deva Ramanan and Simon Baker. Local distance functions: A taxonomy, new algorithms, and an evaluation. *IEEE Transactions on Pattern Analysis and Machine Intelligence*, 33(4):794–806, 2010.

[31] Sachin Ravi and Hugo Larochelle. Optimization as a model for few-shot learning. In *5th International Conference on Learning Representations, ICLR 2017, Toulon, France, April 24-26, 2017, Conference Track Proceedings*, 2017. URL <https://openreview.net/forum?id=rJY0-Kc11>.

[32] Mengye Ren, Eleni Triantafillou, Sachin Ravi, Jake Snell, Kevin Swersky, Joshua B. Tenenbaum, Hugo Larochelle, and Richard S. Zemel. Meta-learning for semi-supervised few-shot classification. *CoRR*, abs/1803.00676, 2018. URL <http://arxiv.org/abs/1803.00676>.

[33] James Requeima, Jonathan Gordon, John Bronskill, Sebastian Nowozin, and Richard E Turner. Fast and flexible multi-task classification using conditional neural adaptive processes. *arXiv preprint arXiv:1906.07697*, 2019.

[34] Olga Russakovsky, Jia Deng, Hao Su, Jonathan Krause, Sanjeev Satheesh, Sean Ma, Zhiheng Huang, Andrej Karpathy, Aditya Khosla, Michael Bernstein, et al. Imagenet large scale visual recognition challenge. *International journal of computer vision*, 115(3):211–252, 2015.

[35] Andrei A. Rusu, Dushyant Rao, Jakub Sygnowski, Oriol Vinyals, Razvan Pascanu, Simon Osindero, and Raia Hadsell. Meta-learning with latent embedding optimization. *CoRR*, abs/1807.05960, 2018. URL <http://arxiv.org/abs/1807.05960>.

[36] Victor Garcia Satorras and Joan Bruna Estrach. Few-shot learning with graph neural networks. In *International Conference on Learning Representations*, 2018. URL <https://openreview.net/forum?id=BJj6qGbRW>.

[37] B. Schroeder and Y Cui. Fgvcx fungi classification challenge 2018. [https://github.com/visipedia/fgvcx\\_fungi\\_comp](https://github.com/visipedia/fgvcx_fungi_comp), 2018.

[38] Karen Simonyan and Andrew Zisserman. Very deep convolutional networks for large-scale image recognition. *arXiv 1409.1556*, 09 2014.

[39] Jake Snell, Kevin Swersky, and Richard Zemel. Prototypical networks for few-shot learning. In *Advances in Neural Information Processing Systems*, pages 4077–4087, 2017.

[40] M. Sornam, K. Muthusubash, and V. Vanitha. A survey on image classification and activity recognition using deep convolutional neural network architecture. In *2017 Ninth International Conference on Advanced Computing (ICoAC)*, pages 121–126, Dec 2017. doi: 10.1109/ICoAC.2017.8441512.

[41] Flood Sung, Yongxin Yang, Li Zhang, Tao Xiang, Philip HS Torr, and Timothy M Hospedales. Learning to compare: Relation network for few-shot learning. In *Proceedings of the IEEE Conference on Computer Vision and Pattern Recognition*, pages 1199–1208, 2018.

[42] Christian Szegedy, Wei Liu, Yangqing Jia, Pierre Sermanet, Scott E. Reed, Dragomir Anguelov, Dumitru Erhan, Vincent Vanhoucke, and Andrew Rabinovich. Going deeper with convolutions. *CoRR*, abs/1409.4842, 2014. URL <http://arxiv.org/abs/1409.4842>.

[43] Eleni Triantafillou, Tyler Zhu, Vincent Dumoulin, Pascal Lamblin, Kelvin Xu, Ross Goroshin, Carles Gelada, Kevin Swersky, Pierre-Antoine Manzagol, and Hugo Larochelle. Meta-dataset: A dataset of datasets for learning to learn from few examples. *arXiv preprint arXiv:1903.03096*, 2019.

[44] Oriol Vinyals, Charles Blundell, Timothy Lillicrap, Daan Wierstra, et al. Matching networks for one shot learning. In *Advances in neural information processing systems*, pages 3630–3638, 2016.

[45] Catherine Wah, Steve Branson, Peter Welinder, Pietro Perona, and Serge Belongie. The caltech-ucsd birds-200-2011 dataset. 2011.

[46] Wei Wang, Vincent W. Zheng, Han Yu, and Chunyan Miao. A survey of zero-shot learning: Settings, methods, and applications. *ACM Trans. Intell. Syst. Technol.*, 10(2):13:1–13:37, January 2019. ISSN 2157-6904. doi: 10.1145/3293318. URL <http://doi.acm.org/10.1145/3293318>.

[47] Yaqing Wang and Quanming Yao. Few-shot learning: A survey. *CoRR*, abs/1904.05046, 2019. URL <http://arxiv.org/abs/1904.05046>.

[48] Kilian Q Weinberger and Lawrence K Saul. Distance metric learning for large margin nearest neighbor classification. *Journal of Machine Learning Research*, 10(Feb):207–244, 2009.

[49] Jason Yosinski, Jeff Clune, Yoshua Bengio, and Hod Lipson. How transferable are features in deep neural networks? *CoRR*, abs/1411.1792, 2014. URL <http://arxiv.org/abs/1411.1792>.

## A Benchmarks and Training

### A.1 Meta-Dataset

A brief description of the sampling procedure used in the Meta-Dataset setting is already provided in Section 4.1. This sampling procedure, however, comes with additional specifications that are uniform across all tasks (such as count enforcing) and dataset specific details such as considering the class hierarchy in ImageNet tasks. The full algorithm for sampling is outlined in [43], and we refer the interested reader to Section 3.2 in [43] for complete details. This procedure results in a task distribution where most tasks have fewer than 10 classes and each class has fewer than 20 support examples. The task frequency relative to the number of classes is presented in Figure 5a, and the class frequency as compared to the class shot is presented in Figure 5b. The query set contains between 1 and 10 (inclusive) examples per class for all tasks; fewer than 10 query examples occur only when there are not enough total images to support 10 query examples.

### A.2 mini/tiered-ImageNet

Task sampling across both mini-ImageNet and tiered-ImageNet first starts by defining a constant number of ways and shots that will be used for each generated task. For a  $L$ -shot  $K$ -way problem setting, first  $K$  classes are sampled from the dataset with random probability. Then, for each sampled class,  $L$  of the class images are sampled with random probability and used as the support examples for the class. In addition, 10 query images (distinct from the support images) are sampled per class.

### A.3 Meta-Dataset Training/Testing

Following [1; 33], we train using Episodic training [39; 6] where tasks themselves are used as training examples. For each iteration of Episodic training, a task (with additional ground truth query labels) is generated, and the adaptation network is trained to minimize the classification error (cross entropy) of the query set given the task. The pre-trained ResNet18 feature extractor is fixed during this process. We train for a total of 110K tasks, with 16 tasks per batch, resulting in 6875 gradient updates. We train using Adam optimizer with learning rate of  $5 \times 10^{-4}$ . We evaluate on the validation splits of all 8 in-domain and 1 out-of-domain (MSCOCO) datasets, saving the best performing checkpoint for test-time evaluation.

### A.4 mini/tiered-ImageNet Training/Testing

Similar to Meta-Dataset, we use Episodic training: at each iteration, a task is generated, and we backpropagate the query set classification loss through the adaptation network. For mini/tiered-ImageNet, we train for a total of 20K tasks, validating performance every 2K tasks and saving the best checkpoint for test-time evaluation. We, similarly, use the Adam optimiser with learning rate of  $5 \times 10^{-4}$ , and use a batch size of 16, for a total of 1250 gradient steps.

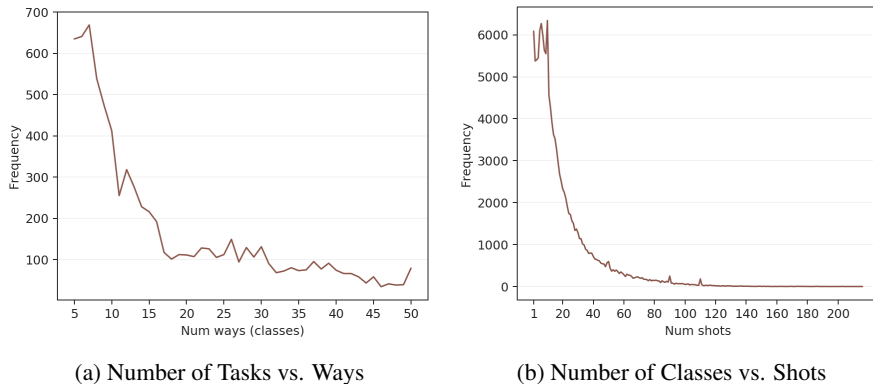


Figure 5: Test-time way and shot frequency graphs. Figure is directly from [1]. As shown, most tasks have fewer than 10 classes (way) and most classes have less than 20 support examples (shot).

## B mini/tiered-ImageNet Baselines

Past state of the art methods and their performances on mini-ImageNet and tiered-ImageNet on 1/5-shot 5/10-way few-shot visual classification are shown in Table 6. We must emphasize that CNAPS-based models, including ours, use a ResNet18 feature extractor pre-trained on ImageNet. This gives CNAPS-derived methods an unfair advantage over past baselines. We provide these baselines for reference and discourage drawing strong direct comparisons between them and CNAPS-derived methods.

Model	mini-ImageNet Accuracy (%)				tiered-ImageNet Accuracy (%)			
	5-way		10-way		5-way		10-way	
	1-shot	5-shot	1-shot	5-shot	1-shot	5-shot	1-shot	5-shot
MAML [6]	48.7±1.8	63.1±0.9	31.3±1.1	46.9±1.2	51.7±1.8	70.3±1.7	34.4±1.2	53.3±1.3
MAML+ [22]	50.8±1.8	66.2±1.8	31.8±0.4	48.2±1.3	53.2±1.8	70.8±1.8	34.8±1.2	54.7±1.3
Reptile [26]	47.1±0.3	62.7±0.4	31.1±0.3	44.7±0.3	49.0±0.2	66.5±0.2	33.7±0.3	48.0±0.3
Reptile+BN [26]	49.9±0.3	66.0±0.6	32.0±0.3	47.6±0.3	52.4±0.2	71.0±0.2	35.3±0.3	52.0±0.3
ProtoNet [39]	46.1±0.8	65.8±0.7	32.9±0.5	49.3±0.4	48.6±0.9	69.6±0.7	37.3±0.6	57.8±0.5
RelationNet [41]	51.4±0.8	67.0±0.7	34.9±0.5	47.9±0.4	54.5±0.9	71.3±0.8	36.3±0.6	58.0±0.6
Gidaris et al. [8]	56.2±0.9	73.0±0.6	NA	NA	NA	NA	NA	NA
TADAM [28]	58.5±0.3	76.7±0.3	NA	NA	NA	NA	NA	NA
TPN [22]	51.4±0.8	67.1±0.7	34.9±0.5	47.9±0.4	59.9±0.9	73.3±0.7	44.8±0.6	59.4±0.5
LEO [35]	61.8±0.1	77.6±0.1	NA	NA	66.3±0.1	81.4±0.1	NA	NA
CNAPS [33]	77.8±1.0	87.6±0.7	65.7±0.7	80.0±0.6	75.7±1.0	85.5±0.7	63.7±0.7	78.2±0.5
Simple CNAPS [1]	80.5±0.9	89.5±0.6	68.6±0.7	83.7±0.5	79.0±0.9	87.6±0.6	67.1±0.7	81.0±0.5
Transductive CNAPS	<b>82.4±0.9</b>	<b>90.9±0.5</b>	<b>73.3±0.7</b>	<b>85.7±0.5</b>	<b>81.0±0.9</b>	<b>89.2±0.6</b>	<b>69.1±0.7</b>	<b>83.1±0.5</b>

Table 6: Few-shot visual classification results on 1/5-shot 5/10-way few-shot on mini/tiered-ImageNet. Note that unlike Table 3, we also present baselines here. **We emphasize that direct comparisons of these results with CNAPS-based models should be avoided due to CNAPS-based methods using a ResNet18 feature extractor pre-trained on ImageNet.**

## C Connections with Riemannian metric learning

Here, we frame the Simple CNAPS and Transductive CNAPS family of models in a Riemannian metric learning framework.

Riemannian metric learning seeks to learn an underlying local *metric tensor* ( $d \times d$  positive-definite matrix defined for each point in  $\mathbb{R}^d$ ),  $\mathbf{g}(\mathbf{x})$ , in a data or feature space  $\mathbb{R}^d$ . The metric tensor defines the geometry of the underlying space; in particular, we can use it to define a notion of length. The distance along a path  $\gamma : [0, 1] \rightarrow \mathbb{R}^d$  is computed in terms of this metric tensor via the arclength functional:

$$\mathcal{L}[\gamma] = \int_0^1 \sqrt{\dot{\gamma}(\lambda)^T \mathbf{g}(\gamma(\lambda)) \dot{\gamma}(\lambda)} d\lambda \quad (8)$$

From this, we can derive a global distance metric (the geodesic distance) between points as (loosely) the length of the shortest path between  $\mathbf{x}$  and  $\mathbf{y}$ :

$$d(\mathbf{x}, \mathbf{y}) = \inf_{\gamma} \mathcal{L}[\gamma] \text{ for } \gamma \text{ where } \gamma(0) = \mathbf{x}, \gamma(1) = \mathbf{y} \quad (9)$$

The arclength functional is difficult to analyze, but we can instead analyze the *energy functional*  $E[3]$ :

$$E[\gamma] = \int_0^1 \dot{\gamma}(\lambda)^T \mathbf{g}(\gamma) \dot{\gamma}(\lambda) d\lambda \quad (10)$$

Both  $E$  and  $\mathcal{L}$  yield the same local minimizers; these are called geodesics, and are equivalent to straight lines in the geometry defined by  $\mathbf{g}(\mathbf{x})$ .

In metric learning, our goal is to estimate the metric tensor  $\mathbf{g}(\mathbf{x})$  from data. This is a very underdetermined task, since its only constraints are smoothness and positive definiteness.

To reduce the space of metric tensors under consideration, we treat the class centroids  $\mu_k$  as local inducing points for a metric that is locally (near  $\mu_k$ ) the Mahalanobis distance defined by  $\mathbf{Q}_k$ , and

model the global metric tensor as some smooth interpolation of these local Mahalanobis metrics:

$$\mathbf{g}(\mathbf{x}) = \sum_k w_k(\mathbf{x} - \mu_k) \mathbf{Q}_k^{-1} \quad (11)$$

Here,  $\{w_k(\mathbf{r})\}_k$  is a smooth partition of unity, which satisfies:

$$w_k(\mathbf{0}) = 1 \quad (12)$$

$$w_k(\mathbf{x}) \geq 0 \quad (13)$$

$$\sum_k w_k(\mathbf{x}) = 1 \quad (14)$$

The existence of such functions is guaranteed [20].

Even with these simplifying assumptions, the global geodesic distance is extremely challenging to compute in high dimensions. Since the geodesic distance is the minimum path length over all paths, we can upper bound it by a specific path [30]:

$$d(\mathbf{x}, \mathbf{y}) \leq \int_0^1 \sqrt{\dot{\mathbf{c}}(\lambda)^T \mathbf{g}(\mathbf{c}(\lambda)) \dot{\mathbf{c}}(\lambda)} d\lambda \quad (15)$$

where  $\mathbf{c}(\lambda) = (1 - \lambda)\mathbf{x} + \lambda\mathbf{y}$  is a straight line (in the coordinate space) interpolation. The time derivative of  $\mathbf{c}$  is easily computed to be  $\dot{\mathbf{c}} = \mathbf{y} - \mathbf{x}$ .

The corresponding energy functional upper bounds the squared distance:

$$d(\mathbf{x}, \mathbf{y})^2 \leq \tilde{E}(\mathbf{x}, \mathbf{y}) = \int_0^1 \dot{\mathbf{c}}(\lambda)^T \mathbf{g}(\mathbf{c}(\lambda)) \dot{\mathbf{c}}(\lambda) d\lambda \quad (16)$$

We don't actually care too much about the actual squared distance for purposes of classification - we care about the difference in distance between a test point  $\mathbf{x}$  and two class centroid  $\mu_i, \mu_j$ , which corresponds to their relative probabilities. Substituting the energy along the straight-line paths yields:

$$\Delta E_{ij} = \tilde{E}(\mathbf{x}, \mu_i) - \tilde{E}(\mathbf{x}, \mu_j) = \int_0^1 \Delta_i^T \mathbf{g}_i(\lambda) \Delta_i - \Delta_j^T \mathbf{g}_j(\lambda) \Delta_j d\lambda \quad (17)$$

where:

$$\Delta_k = (\mathbf{x} - \mu_k) \quad (18)$$

$$\mathbf{g}_k(\lambda) = \mathbf{g}(\lambda\mu_k + (1 - \lambda)\mathbf{x}) \quad (19)$$

We can write  $\Delta E_{ij}$  in terms of a path parameter  $T \in [0, \frac{1}{2}]$  as:

$$\Delta E_{ij}(T) = \int_0^T \Delta_i^T \mathbf{g}_i(\lambda) \Delta_i - \Delta_j^T \mathbf{g}_j(\lambda) \Delta_j d\lambda + \int_{1-T}^1 \Delta_i^T \mathbf{g}_i(\lambda) \Delta_i - \Delta_j^T \mathbf{g}_j(\lambda) \Delta_j d\lambda \quad (20)$$

As  $T$  increases, we simultaneously grow the path inward from each class centroid towards  $\mathbf{x}$  and outward from  $\mathbf{x}$  to the class centroids.

A first-order Taylor expansion of this around  $T = 0$  causes the first integral to drop out (since  $g_i(0) = g_j(0)$ ), and the second integral yields (when evaluated at  $T = \frac{1}{2}$ ):

$$\Delta E_{ij} \approx \frac{1}{2} [(\mathbf{x} - \mu_i)^T \mathbf{Q}_i^{-1} (\mathbf{x} - \mu_i) - (\mathbf{x} - \mu_j)^T \mathbf{Q}_j^{-1} (\mathbf{x} - \mu_j)] \quad (21)$$

The higher order terms can be controlled to some degree by forcing the partition functions  $w_k(\mathbf{x})$  are very flat near the class centroids.

This allows us to think of the Simple CNAPS classifier logit function (squared Mahalanobis distance to class centroids with per-class metrics) as a coarse approximation of the geodesic energy between a test point and a class centroid; this coarse approximation is improved slightly by noting that other low-order terms that could be considered drop out when examining the *difference* in geodesic energy between a test point and two class centroids.

This fits into an energy-based classification framework[9], where the energy function describing the joint energy of a point  $\mathbf{x}$  in feature space (with the structure of a Riemannian manifold) and a class  $y$  is given by:

$$H(\mathbf{x}, y) = \inf_{\gamma: \gamma(0) = \mathbf{x}, \gamma(1) = \mu_y} E[\gamma] \quad (22)$$

where  $\mu_y$  are class prototype points on the same manifold; in other words, the joint energy of a class, instance pair is given by the geodesic energy connecting that instance with some prototype instance of the target class.